Biosensors and Bioelectronics 177 (2021) 112948

Contents lists available at ScienceDirect

Biosensors and Bioelectronics

journal homepage: http://www.elsevier.com/locate/bios

Deconvolution of WNT-induced Frizzled conformational dynamics with fluorescent biosensors

Hannes Schihada [a], Maria Kowalski-Jahn [a], Ainoleena Turku [a,b], Gunnar Schulte [a,*]

[a] Section of Receptor Biology & Signaling, Department of Physiology & Pharmacology, Karolinska Institutet, S-17165, Stockholm, Sweden
[b] Computational Medicine Design Unit; Orion Corporation Orion Pharma; P.O.Box 65 (Orionintie 1); FI-02101 Espoo, Finland

ARTICLE INFO

Keywords:
WNT
Frizzled
Conformational biosensor
Activation mechanism
Ligand selectivity
Drug screening

ABSTRACT

The G protein-coupled receptors Frizzled$_{1\text{-}10}$ (FZD$_{1\text{-}10}$) act as molecular checkpoints mediating intracellular signaling induced by 19 mammalian, secreted Wingless/Int-1 lipoglycoproteins (WNTs). Despite the vital roles of these signaling components in health and disease, our knowledge about WNT/FZD selectivity, and the mechanisms of receptor activation and intracellular signal propagation by individual ligand/receptor pairs is limited due to the current lack of suitable biophysical techniques. Here, we developed fluorescence-based biosensors that detect WNT-induced FZD conformational changes in living cells in order to assess WNT action via FZDs at the most proximal level, i.e. the receptor conformation. By testing a panel of recombinant ligands on conformational biosensors representing all four homology clusters of FZDs, we discover yet unappreciated selectivities of WNTs to their receptors and, surprisingly, identify distinct ligand-induced receptor conformations. Furthermore, we demonstrate that FZDs can undergo conformational changes upon WNT binding without being dependent on the WNT co-receptors LRP5/6. This sensor toolbox provides an advanced platform for a thorough investigation of the 190 possible WNT/FZD pairings and for future screening campaigns targeting synthetic FZD ligands. Furthermore, our findings shed new light on the complexity of the WNT/FZD signaling system and have substantial implications for our understanding of fundamental biological processes including embryonal development and tumorigenesis.

1. Introduction

Frizzleds (FZDs) are evolutionarily conserved transmembrane receptors and belong to the Class F of G protein-coupled receptors (GPCRs) (Schulte, 2010). FZDs bind 19 mammalian, secreted lipoglycoproteins of the Wingless/Int-1 family (WNTs) via their extracellular cysteine-rich domain (CRD) (Grainger and Willert, 2018). This binding process is seen as the primary event initiating WNT morphogen signaling through the scaffold protein disheveled 1, 2 or 3 (DVL1-3), feeding, most prominently, into the WNT/β-catenin pathway, but also into β-catenin-independent cascades (e.g. WNT/Ca^{2+}, WNT/RAC, WNT/RHO or WNT/planar-cell-polarity (PCP)-like pathways) (Clevers and Nusse, 2012; Semenov et al., 2007; Yang and Mlodzik, 2015). Furthermore, accumulating evidence over the last years has highlighted the role of heterotrimeric G proteins (Bowin et al., 2019; Schulte and Wright, 2018; Wright et al., 2019) and β-arrestins (Bryja et al., 2007, 2008; Kim et al., 2008), acting as intracellular signal transducers that mediate DVL-independent WNT/FZD signaling. Given the vital role of WNT signaling in stem cell biology, embryonic development and tumorigenesis (Nusse and Clevers, 2017), it is obvious that we need to attain a deeper mechanistic understanding of the WNT/FZD signaling system in order to develop innovative, therapeutic strategies targeting selected ligand/receptor pairs in a mechanism-based manner. These novel therapies should ideally modulate WNT/FZD signaling in a subtype- and pathway-selective manner without affecting disease-unrelated ligand/receptor pairs that maintain physiological WNT signaling.

The Class F of GPCRs is composed of ten closely related receptors, named FZD$_{1\text{-}10}$, and an ancestral member called Smoothened (SMO). SMO does not bind WNTs, but mediates hedgehog signaling. FZD$_{1\text{-}10}$ are further sub-grouped into four homology clusters (FZD$_{1,2,7}$/FZD$_{3,6}$/FZD$_{4,9,10}$/FZD$_{5,8}$) (Schulte, 2010). So far it remains enigmatic, if and how the 19 mammalian WNTs exert FZD subtype selectivity and whether signaling of specific WNT/FZD pairings shows any degree of functional selectivity (Dijksterhuis et al., 2015; Kilander et al., 2011;

* Corresponding author.
E-mail addresses: hannes.schihada@ki.se (H. Schihada), maria.kowalski.jahn@ki.se (M. Kowalski-Jahn), ainoleena.turku@ki.se (A. Turku), gunnar.schulte@ki.se (G. Schulte).

https://doi.org/10.1016/j.bios.2020.112948
Received 9 November 2020; Accepted 25 December 2020
Available online 30 December 2020

Schulte, 2015). Furthermore, the structural and mechanistic basis of WNT signaling through FZDs motivates an ongoing and intense matter of debate. The fundamental question is whether (a) WNT binding to FZDs promotes intracellular signaling exclusively by cross-linking FZDs with so-called WNT co-receptors in signalosomes, or (b) whether ligand engagement with the CRD initiates allosterically co-receptor-independent conformational changes within FZDs. These rearrangements are then converted to FZD/transducer coupling and intracellular signal propagation. The former concept is widely accepted for the β-catenin pathway, which originates from WNT-mediated FZD/LRP5/6 signalosome formation (Bilic et al., 2007; DeBruine et al., 2017; Hua et al., 2018; Janda et al., 2012; Tsutsumi et al., 2020). The latter, in contrast, is reminiscent of what is known for the activation of class A and B GPCRs where extracellular ligand engagement allosterically promotes receptor/effector coupling at the intracellular side. This concept has been established in the late 70s and early 80s as the ternary complex model and accumulating evidence argues that it is also applicable to Class F receptors (De Lean et al., 1980; Schulte and Wright, 2018). In fact, recent studies provided important evidence supporting this notion of WNT-induced conformational dynamics in FZDs (Kozielewicz et al., 2019, 2020; Wright et al., 2018, 2019; Yang et al., 2018).

In order to assess ligand/receptor selectivity, WNT/FZD interaction was previously inferred through seminal work in models of *Drosophila melanogaster* by employing signaling-dependent and highly amplified readouts (Bhanot et al., 1996; Hsieh et al., 1999; van Amerongen et al., 2008; Wu and Nusse, 2002). Subsequent studies applied similar strategies to map WNT/FZD combinations in mammalian test systems (Voloshanenko et al., 2017; Yu et al., 2012). These approaches, however, (a) disregard the diverse signaling portfolio of WNT/FZD complexes through β-catenin-independent pathways, (b) cannot distinguish individual WNT/FZD pairings in presence of ubiquitously expressed WNT receptors, and (c) are sensitive to signaling crosstalk and interference by the pluridimensional regulation of WNT signaling (Garcia de Herreros and Dunach, 2019). In contrast to these signaling-dependent assays, previous biochemical studies assessed WNT/FZD selectivity using purified FZD CRDs and reported binding affinities ranging from 1 to 100 nM (Dijksterhuis et al., 2015; Hsieh et al., 1999). While offering the most proximal readout of ligand/receptor interaction, this biochemical setting excludes the (putative) modulatory role of the receptor's transmembrane core and does not recapitulate the natural environment of these interactions on the surface of living cells. In contrast, an important progress has been achieved recently with the development of fluorescently-labeled WNT-3A and its application in bioluminescence-resonance-energy-transfer (BRET) experiments with NanoLuciferase-tagged, full-length FZD_4 (Wesslowski et al., 2020). While this approach offers a very promising platform to investigate family-wide binding of WNTs to FZDs in living cells, its throughput is limited by the tedious purification of labeled WNTs, which are not commercially available, and, moreover, no conclusions can be drawn with respect to receptor conformational dynamics.

In light of the remaining discourse about ligand/receptor selectivity and receptor activation mechanisms, it is obvious that we are in need of advanced biophysical tools to examine these underlying details of WNT signaling through FZDs. Furthermore, the involvement of FZDs in numerous diseases (Wang et al., 2016) and their druggability with small molecule compounds (Blagodatski et al., 2014; Kozielewicz et al., 2020) underlines the requirements for screening-compatible assays that are able to detect FZD-targeting compounds in an unbiased (i.e. signaling pathway-independent) fashion (Koval and Katanaev, 2012).

In order to address these limitations, we developed a set of conformational receptor biosensors representing all four FZD homology clusters. These biosensors are based on a conformationally sensitive green fluorescent protein inserted between the receptors' transmembrane helices 5 and 6 (TM5/6). This approach does not only allow us to infer WNT/FZD selectivity to full length receptors in living cells, but also sheds light on the role of FZD/WNT co-receptor interplay and uncovers unique patterns of ligand-induced conformational changes in FZDs in a medium-throughput assay format.

2. Material and methods

2.1. Reagents

Recombinant WNT-3A (# 5036-WN-010), WNT-5A (# 645-WN-010), WNT-5B (# 7347-WN-025), WNT-7A (# 3008-WN-025), WNT-10B (# 7196-WN-010), WNT-11 (# 6179-WN-010), WNT-16B (# 7790-WN-025) and DKK1 (# 5439-DK-010/CF) were purchased from R&D systems/Biotechne. NanoLuciferase substrate furimazine (#N1572) and HaloTag® NanoBRET™ 618 Ligand (#G9801) were provided by Promega. C59 (2-[4-(2-Methylpyridin-4-yl)phenyl]-N-[4-(pyridin-3-yl)phenyl]acetamide) porcupine inhibitor was from Abcam (# ab142216). Lipofectamine 2000 transfection reagent, Phusion Polymerase and Geneart™ site-directed mutagenesis kit (# A13312) were purchased from Thermo Fisher Scientific. Dulbecco's Modified Eagle's Medium (DMEM) and G-418 (Geneticin) were from Gibco. Sigmacote, ECM Gel from Engelbreth-Holm-Swarm murine sarcoma and 3-[(3-cholamidopropyl)dimethylammonio]-1-propanesulfonate (CHAPS) were from Sigma Aldrich. F-bottom, white-wall, white-bottomed and black-wall, black-bottomed 96-well plates were from Greiner BioOne. HEK293 cells (# CRL-1573) were purchased from ATCC. pCMV-dLight1.1 was a gift from Lin Tian (Addgene plasmid #111053; http://n2t.net/addgene:111,053; RRID:Addgene 111,053).

2.2. Cell culture, transient transfection and generation of stable cell lines

Human embryonic kidney cells (HEK293A) and $\Delta FZD_{1\text{-}10}$ HEK293 cells (Eubelen et al., 2018) were used for transient expression and grown in DMEM supplemented with 10% fetal calf serum, 0.1 mg/mL streptomycin, and 100 units/mL penicillin at 37 °C with 5% CO_2. All transfections were performed using Lipofectamine 2000 in a 2 μL Lipofectamine 2000/μg total DNA ratio. For the generation of stable $FZD_{4/5/6/7}$-cpGFP sensor cell lines, HEK293A cells grown in T75 flasks were transfected at a confluence of 40–50% with 1 μg of DNA. To select for stably expressing cells, transfected cells were cultured with 2000 μg/mL of G-418 and maintained in DMEM supplemented with 500 μg/mL G-418, 10% fetal calf serum, 0.1 mg/mL streptomycin, and 100 units/mL penicillin at 37 °C with 5% CO_2.

2.3. Building homology models of FZDs and 3D structural alignment

The amino acid sequences of FZD_5 (UniProt ID: Q13467), FZD_6 (UniProt ID: O60353) and FZD_7 (UniProt ID: O75084) were aligned to those of FZD_4 (PDB ID: 6BD4) (Yang et al., 2018) and SMO (PDB IDs: 5L7D and 4QIN) (Byrne et al., 2016; Wang et al., 2014) with ClustalX2 (Larkin et al., 2007). Homology modelling was conducted with MODELLER 9.19 (Webb and Sali, 2014) in batches of 20 models and alignments were manually edited in course of the modelling process to ensure the proper locations of the seven transmembrane (7TM) domains, conserved Class F GPCR motifs and essential cysteine residues (Valnohova et al., 2018) corresponding to the disulphide bridges Cys193-Cys213 and Cys217-Cys295 (amino acid numbering as in SMO). FZD_4 crystal structure served as a main template for the 7TM core and intracellular loops, whereas SMO structures were used for modelling the extracellular loops and the extension of TM6. The representative models were picked among the final 20 models based on their DOPE scores (Shen and Sali, 2006).

2.4. Cloning of FZD constructs

To clone BRET-based FZD_4 conformational biosensors, HaloTag was amplified from $\alpha_{2A}AR_{Nluc/HaloTag}$ (Schihada et al., 2018) and inserted in the indicated positions of intracellular loop 2 and 3 of FZD_4-Nluc. All

cpGFP-based conformational sensors were cloned by amplifying LSSLI-cpGFP-NHDQL from dLight1.1 (Patriarchi et al., 2018) and inserting it to the indicated positions in the human templates of FZD_{4-7}. To remove C-terminal tags in FZD-cpGFP constructs, a stop codon was fused to the last base triplet of the template receptor constructs. All gene insertions were performed employing prolonged overlap extension PCR techniques with high-fidelity Phusion polymerase (ThermoFisher) and the Geneart™ site-directed mutagenesis kit (ThermoFisher) was used to insert C-terminal stop codons.

2.5. Confocal microscopy

The day prior transfection, 80,000 HEK293A cells/well were seeded into extracellular matrix (ECM; Sigma)-pre-coated 4-chamber plates. Adherent cells were transfected with 500 ng $FZD_{4/5/6/7}$-cpGFP per well and grown overnight. About 24 h after transfection, cells were washed in DPBS, kept in 0.1% BSA/HBSS and imaged using a Zeiss LSM710 confocal microscope.

2.6. Handling of recombinant WNT preparations and dickkopf-1

Lyophilized preparations of recombinant WNTs and DKK1 were dissolved in 0.1% BSA/DPBS to obtain a stock solution of 100 μg/mL and stored at 4–8 °C for maximum 4 weeks. Depending on the batch, the WNT stock solutions contained 0.04–0.10 mM EDTA, 0.15–0.50% (w/V) CHAPS and 0.15% (w/V) bovine serum albumin. Vehicle control stock solutions were prepared accordingly, sterile filtered and stored at 4–8 °C for maximum 4 weeks. Prior application of recombinant WNTs and DKK1 in cell-based experiments, 10-fold compound dilutions were prepared in 0.1% BSA/DPBS in transparent 96-well plates that were pre-coated with Sigmacote to avoid adsorption of recombinant proteins to plastic surfaces. All pipetting steps were performed with Sigmacote-pre-coated pipette tips.

2.7. Receptor-cpGFP fluorescence measurements

For experiments with transient expression of FZD_4-cpGFP or D_1R-cpGFP, HEK293A cells were transfected in suspension with 1 μg of sensor DNA per mL cell suspension (400,000 cells/mL) and seeded onto black-wall, black-bottomed 96-well microtiter plates. 24 h after transfection, C59 was added to a final concentration of 10 nM. Stable cell lines expressing $FZD_{4/5/6/7}$-cpGFP were resuspended in medium supplemented with 10 nM C59 and seeded the day before experiment onto black-wall, black-bottomed 96-well microtiter plates at a density of 100,000 cells/well. 48 h after transient transfection or 24 h after seeding stable $FZD_{4/5/6/7}$-cpGFP cells, wells were washed with 100 μL Hank's balanced salt solution (HBSS) and incubated with 90 μL of 0.1% bovine serum albumin in HBSS (0.1% BSA/HBSS). Baseline fluorescence was recorded in at least 5 consecutive reads, 10 μl of 10-fold WNT solution, (WNT preparations in 0.1% BSA/HBSS) or vehicle control was applied per well and the resulting fluorescence intensity was recorded for additional 10–20 min. For experiments with destabilized WNT-5A, the 10-fold ligand and vehicle solution were subjected to two cycles of a freeze (1 h at -20 °C)/heat (45 min at 65 °C) treatment prior addition to the sensor cells. To assess the effect of LRP5/6 inhibition on the FZD_4-cpGFP response, stable sensor cells were incubated for 10 min with 1 μg/mL DKK1 or vehicle control prior addition of WNT-3A or vehicle control. All experiments were conducted using a CLARIOstar plate reader (BMG Labtech, Ortenberg, Germany) equipped with filters to excite cpGFP (470/15) and record its emission intensity (515/20 nm). 40 flashes were applied per data point.

2.8. BRET-based comparison of receptor-cpGFP surface expression

HEK293A cells were transiently transfected with 500 ng CD86-Nluc along with 500 ng pcDNA (to control for Nluc bleedthrough into the acceptor emission channel) or GPCR-cpGFP per mL of cell suspension (400,000 cells/mL) and seeded onto PDL-precoated white-wall, white-bottomed 96-well microtiter plates. 10 nM C59 was added to the cells 24 h after transfection. 48 h after transfection, cells were washed once with HBSS and incubated with 100 μL of a 1/1000 dilution of furimazine stock solution in HBSS. Sensor surface expression was measured by means of bystander BRET between Nluc and cpGFP using a CLARIOstar plate reader equipped with monochromators to separate Nluc (450/60 nm) and cpGFP (525/30 nm) emission intensities. The integration time was set to 0.3 s.

2.9. FZD_4-HaloTag/Nluc BRET measurements

For experiments with FZD_4-HaloTag/Nluc sensors, HEK293A cells were transfected in suspension with 1 μg sensor DNA per mL cell suspension (400,000 cells/mL) and seeded onto PDL-precoated white-wall, white-bottomed 96-well microtiter plates. 24 h after transfection, HaloTag NanoBRET 618 fluorescent dye and porcupine inhibitor C59 were added to a final concentration of 50 nM and 10 nM, respectively. 48 h after transfection, cells were washed with 100 μL HBSS/well and incubated with 90 μL of a 1/1000 dilution of furimazine stock solution in 0.1% BSA/HBSS. After incubation for 3 min at 37 °C, the basal BRET ratio was measured in three consecutive reads and 10 μL of a 10 μg/mL WNT-5A solution (in 0.1% BSA/HBSS) or vehicle control was applied per well. Subsequently, the BRET ratio was recorded for additional 20–25 min. All experiments were conducted using a CLARIOstar plate reader equipped with monochromators to separate Nluc (450/50 nm) and HaloTag NanoBRET 618 (620/30 nm) emission intensities. The integration time was set to 0.3 s.

2.10. TOPFlash reporter gene assay

ΔFZD_{1-10} HEK293 cells (500,000 cells/mL) were transfected in suspension with 400 ng M50 Super 8xTOPFlash, 100 ng pRL-TK Luc and 500 ng FZD_X(-cpGFP) per mL and seeded onto PDL-precoated white-wall, white-bottomed 96-well plates (50,000 cells/well). 24 h after transfection, cells were washed with 100 μL HBSS and incubated for 4 h in 90 μL/well of FBS-reduced (0.5%) DMEM supplemented with 10 nM C59. Thereafter, 10 μL of 10 μg/mL recombinant WNTs (in 0.1% BSA/HBSS) or vehicle control were added. For experiments with the LRP5/6 inhibitor DKK1, cells were pre-incubated with 1 μg/mL DKK1 or vehicle control for 10 min prior WNT addition. 24 h after stimulation, cells were washed with HBSS and lysed in 30 μL of Promega's dual luciferase passive lysis buffer (15 min, room temperature). Subsequently, 20 μL luciferase assay reagent (LARII) was added to each well and β-catenin-dependent firefly luciferase (Fluc) intensity was measured using a CLARIOstar microplate reader (580/80 nm; 1 s integration time). Next, 20 μL Stop&Glo Reagent was added to quantify Renilla luciferase (Rluc) emission intensity (480/80 nm; 1 s integration time) to control for variations in cell number and transfection efficiency.

2.11. Statistical analysis

BRET ratios were defined as acceptor emission/donor emission. At least three individual BRET or fluorescence reads were averaged before and after ligand/vehicle addition ($signal_{basal}$ and $signal_{stim}$, respectively). To quantify ligand-induced changes, ΔBRET and Δfluorescence were calculated for each well as a percent over basal ([($signal_{stim}$ – $signal_{basal}$)/$signal_{basal}$] x 100). Subsequently, the average ΔBRET and Δfluorescence of the vehicle control was subtracted. All TOPFlash ratios were defined as emission in the TCF-mediated Firefly luciferase (Fluc) channel/emission in the expression control Renilla luciferase (Rluc) channel. To express the response as an increase over baseline, all Fluc/Rluc ratios were normalized by dividing the average ratio of the respective WNT vehicle control. Data were analyzed using Prism 6 software (GraphPad, San Diego, CA, USA). Data from concentration-

response experiments were fitted using a four-parameter fit. All data are represented as mean ± s.e.m. of at least three independent experiments and statistical differences were assessed using paired or unpaired Student's t-test and One-way ANOVA followed by post-hoc Turkey test as indicated in the figure legends ($p < 0.05$). The 3D structural alignment of the crystal structure of FZD_4 and the representative homology models of each of the other FZD homology clusters (i.e. models of FZD_5, FZD_6 and FZD_7) was conducted and visualized with PyMol 2.0 (The PyMOL Molecular Graphics System, Schrödinger, New York City, NY, USA). Confocal images were processed using ImageJ 1.8 (National Institutes of Health, Bethesda, MD, USA).

3. Results

3.1. Development of a FZD_4 conformational biosensor

In order to assess ligand/receptor selectivity and efficacy in an unbiased, downstream signaling-independent manner, intramolecular FZD biosensors are required to translate WNT-induced receptor conformational changes into detectable signals. Intramolecular sensors based on fluorescence and bioluminescence resonance energy transfer (FRET/BRET) have been employed since 2003 to study receptor dynamics in living cells (Lohse et al., 2012; Vilardaga et al., 2003) – including for FZD_5 and FZD_6 (Kozielewicz et al., 2020; Wright et al., 2018) – and were optimized more recently to enable compound characterization in a high-throughput-compatible assay format (Schihada et al., 2018, 2020). We employed this optimized BRET design and created four distinct versions of conformational FZD_4 biosensors by (a) fusing Nluc to the receptor C-terminus and by (b) inserting a HaloTag in two distinct positions of intracellular loops 2 and 3 (icl2/icl3) (Fig. S1A, G). However, despite substantial energy transfer in the ligand-free receptor state of all sensor versions, only one sensor variant (FZD_4-Halo(E338/A339)/Nluc) displayed a minimal change in BRET upon WNT-5A stimulation in transiently transfected HEK293 cells (Fig. S1). Due to the minimal amplitude of the ligand-response, we applied a different sensor design based on the placement of circularly permutated green fluorescent protein (cpGFP) between transmembrane helices 5 and 6 (TM5/TM6) (Fig. 1A). This approach has recently yielded several class A and B GPCR biosensors for *in vivo* monitoring of receptor activity (Feng et al., 2019; Jing et al., 2018; Patriarchi et al., 2018; Sun et al., 2018). In principle, the ligand-induced conformational change of the receptor evokes refolding of cpGFP, which, in turn, affects its fluorescence properties reflected by an alteration of its emission intensity. We transferred this technology to class F GPCRs and inserted cpGFP, flanked by the optimized linker sequences LSSLI (N-terminal) and NHDQL (C-terminal) developed by Patriarchi et al., into two distinct sites of FZD_4 (Patriarchi et al., 2018). Based on sequence alignments of FZD_4 to established class A GPCR-cpGFP biosensors (Patriarchi et al., 2018) we selected the amino acids K415/R432 (thereby removing amino acids 416–431) and S418/E431 (removing amino acids 419–430) as insertion sites for cpGFP in FZD_4. As illustrated in Fig. 1B–D, stimulation with recombinant WNT-5A induced an increase in cpGFP emission of both transiently expressed FZD_4 biosensors in living cells in a 96-well microtiter plate format. Mirroring the responses obtained with class A and B biosensors, our results indicate a structural rearrangement within FZD_4 that promotes a conformational change in the fluorescent protein and a subsequent improvement of its photophysical properties. The analogous design of our and previous class A and B receptor sensors with cpGFP placed in icl3, suggests a ligand induced swing out of TM6 as a key mechanism of WNT-induced FZD activation. Indeed, this assumption is supported by previous data using FZD_5 and FZD_6 FRET probes and mini G proteins as sensors of the active conformation of class F receptors, as well as by the crystal structure of active, G protein-bound SMO (Kozielewicz et al., 2020; Qi et al., 2019, 2020; Wright et al., 2018, 2019).

In order to improve assay reproducibility and practicability, we created a HEK293 cell line stably expressing the FZD_4 biosensor version which showed a more stable fluorescence increase upon WNT stimulation (K415-cpGFP-R432) (compare Fig. 1B and C), and controlled for its localization at the cell surface (Fig. S2A-E). Furthermore, in line with the abolished signaling capacity of class A GPCR-cpGFP sensors (Feng et al., 2019; Patriarchi et al., 2018; Sun et al., 2018), insertion of the fluorescent protein abrogated FZD-mediated β-catenin signaling, allowing these sensors to be expressed in biological test systems without interfering with endogenous signaling components (Fig. S2F). To verify the specificity of the FZD_4 sensor for WNT stimulation, we first treated the negative control dopamine D_1 receptor (D_1R)-cpGFP sensor dLight1.1 (Patriarchi et al., 2018) with increasing concentrations of WNT-5A and did not detect any change in fluorescence (Fig. 2A). Secondly, we subjected the recombinant WNT-5A preparation to heat/freeze destabilization prior application to cells stably expressing FZD_4-cpGFP. This treatment abolished the FZD_4-cpGFP response and confirms the dependence of the conformational response on WNT/FZD engagement (Fig. 2B).

3.2. Mechanistic insights to WNT-induced FZD_4 dynamics

While WNT-5A signals primarily through DVL-dependent but β-catenin-independent and heterotrimeric G protein-mediated pathways, WNT-3A is considered the main mediator of FZD/β-catenin signaling (Fig. 3A). Since functional selectivity towards distinct signaling pathways of class A GPCRs is known to be a consequence of specific receptor conformations (Kozielewicz et al., 2019; Smith et al., 2018; Wright et al., 2019), we aimed to evaluate whether FZD_4-cpGFP also detects receptor activation upon engagement of functionally distinct ligands such as WNT-3A and WNT-5A. Therefore, we stimulated the stable cell line with WNT-3A or WNT-5A and recorded the resulting fluorescence response of FZD_4-cpGFP over time (Fig. 3B). Both WNTs induced a distinct and rapid

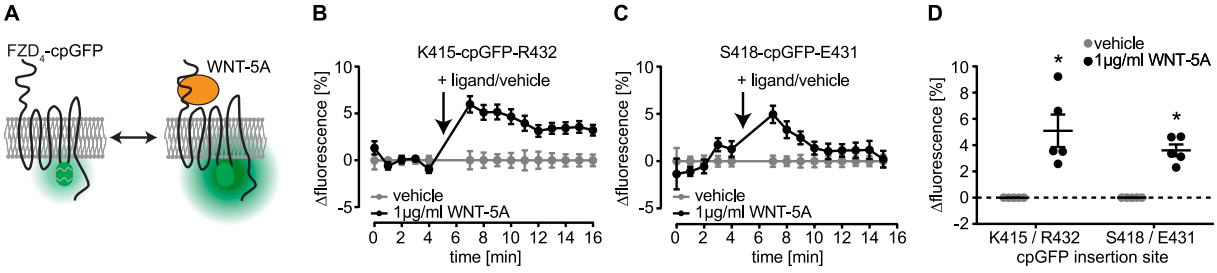

Fig. 1. Development of a conformational FZD_4 biosensor. (**A**) Schematic presentation of the FZD_4-cpGFP biosensor design detecting ligand-induced receptor conformational changes. (**B–C**) Fluorescence time-course response of two distinct FZD_4-cpGFP biosensors upon stimulation with WNT-5A recorded in a 96-well microtiter format. (**D**) Peak response induced by 1 µg/mL WNT-5A on the FZD_4-cpGFP sensors. All experiments were performed using HEK293A cells transiently expressing the indicated FZD_4-cpGFP biosensor versions. Data show mean ± s.e.m. of three to five independent experiments. Statistical significance in (D) was tested applying paired two-way ANOVA followed by Sidak's multiple comparison test against the respective vehicle control. $p < 0.05$.

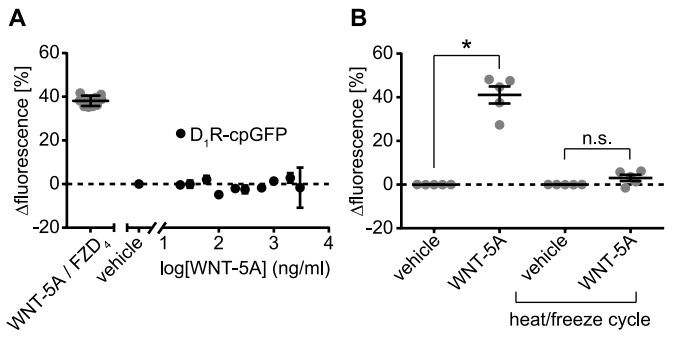

Fig. 2. Validation of the conformational FZD_4 biosensor. (**A**) Response of 3 μg/mL WNT-5A on FZD_4-cpGFP (grey) and concentration-response curve of WNT-5A on D_1R-cpGFP (black). (**B**) Change in FZD_4-cpGFP fluorescence upon stimulation with untreated or heat/freeze subjected 3 μg/mL WNT-5A. All experiments were performed using HEK293A cells stably expressing FZD_4-cpGFP or transiently expressing D_1R-cpGFP. Data show mean ± s.e.m. of three to five independent experiments. Statistical significance in (B) was tested applying paired two-way ANOVA followed by Sidak's multiple comparison test against the respective vehicle control. $p < 0.05$. Mechanistic insights to WNT-induced FZD_4 dynamics.

increase in cpGFP fluorescence compared to vehicle control. These data confirm the suitability of FZD_4-cpGFP to monitor receptor conformations irrespective of the downstream signaling profile mediated by the WNT/FZD pair. Of note, the response of FZD_4-cpGFP emerged with a similar time-course as recorded with a small molecule agonist-stimulated histamine H_3 receptor (H_3R) conformational sensor in a very similar assay format (Schihada et al., 2020). Thus, we propose that this technology opens up the possibility for kinetic studies of FZD activation and medium to high content screening using these cpGFP-based sensors.

As illustrated in Fig. 3A, WNT-3A/β-catenin signaling depends on ligand-mediated association of FZDs with low-density lipoprotein receptor-related protein 5 or 6 (LRP5/6), a process that is blocked by the negative regulator Dickkopf 1 (DKK1). Signal transduction through other, β-catenin-independent pathways often involves the engagement of other WNT co-receptors including adhesion G protein-coupled receptor A2 (ADGRA2/GPR124), Reversion-inducing cysteine-rich protein with Kazal motifs (RECK) and tyrosine-protein kinase transmembrane receptors RYK, PTK7 and ROR1/2 (Eubelen et al., 2018; Grumolato et al., 2010). A current matter of debate is, however, whether WNTs also promote conformational rearrangements in FZDs independently of co-receptors such as LRP5/6. We utilized FZD_4-cpGFP to assess whether the receptor's conformational change upon WNT-3A binding depends on an intermolecular interaction of FZD_4 with LRP5/6. Intriguingly, the WNT-3A-induced response of FZD_4-cpGFP was not affected by pre-incubation with recombinant DKK1 (Fig. 3C and D), used at a concentration that completely abrogates WNT-3A-induced and FZD_4/LRP5/6-mediated β-catenin signaling in FZD_4-transfected FZD_{1-10} KO cells (Fig. 3E). These findings demonstrate that the WNT-3A-mediated fluorescence response in FZD_4-cpGFP reflects an intramolecular receptor rearrangement, which does not require WNT co-receptor involvement, and is reminiscent of conformational dynamics established for class A and B GPCRs.

3.3. *Validation of $FZD_{5/6/7}$-cpGFP biosensors*

In order to study WNT/FZD selectivity and WNT-induced

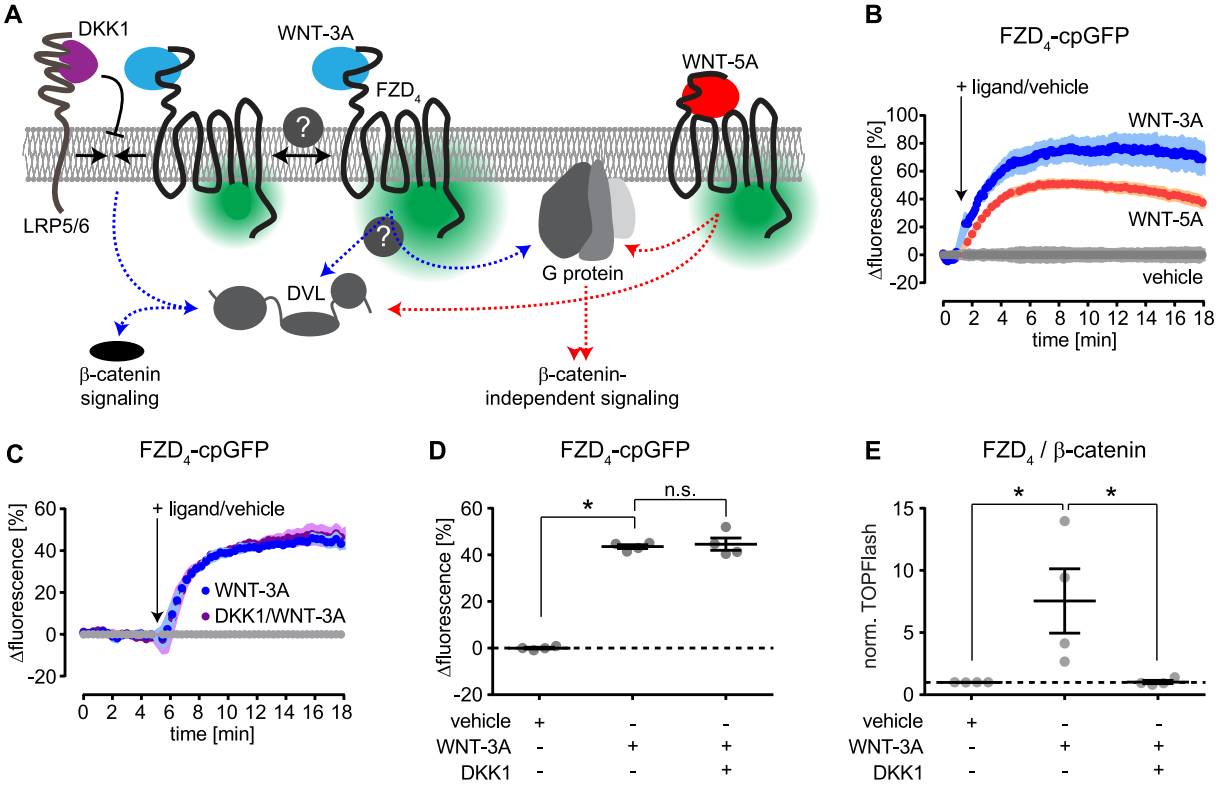

Fig. 3. Mechanistic insights to WNT-induced FZD dynamics. (**A**) Schematic of FZD-dependent signaling pathways mediated by WNT-3A and WNT-5A. (**B**) Time-course fluorescence response induced by 3 μg/mL WNT-3A and 3 μg/mL WNT-5A on FZD_4-cpGFP. (**C**) Change in FZD_4-cpGFP fluorescence upon stimulation with 3 μg/mL WNT-3A in presence or absence of 1 μg/mL DKK1. Experiments in (A–C) were performed using HEK293A cells stably expressing FZD_4-cpGFP. (**D**) TOPFlash reporter gene response induced by 1 μg/mL recombinant WNT-3A in the presence or absence of 1 μg/mL DKK1 in ΔFZD_{1-10} HEK293 cells transiently transfected with FZD_4 wildtype. Data show mean ± s.e.m. of four independent experiments. Statistical significance in (C) and (D) was tested applying One-way ANOVA followed by post-hoc Turkey test.

conformational dynamics at all four FZD homology clusters, we designed and validated cpGFP-based sensors for FZD_5 (cluster $FZD_{5/8}$), FZD_6 ($FZD_{3/6}$) and FZD_7 ($FZD_{1/2/7}$). We selected the equivalent insertion sites to K415/R432 in FZD_4 through structure-based alignment (Fig. S3), confirmed the surface expression of these fusion constructs at the plasma membrane (Fig. S2E) and generated HEK293 cells stably expressing each of these conformational biosensors. All four cpGFP sensors successfully responded to WNT-3A treatment, generating a distinct and rapid fluorescence increase ranging from 20% for FZD_7-cpGFP to about 80% for FZD_5-cpGFP (Fig. 4). Of note, the lower signal amplitudes obtained with FZD_6-and FZD_7-cpGFP resembled their poor surface expression levels relative to their total cellular occurrence (Fig. S2C, D, E), indicating that the high background fluorescence caused by sensors that are not accessible to extracellular WNTs – at least in part – accounts for the smaller Δfluorescence values and lower signal-to-noise ratios.

3.4. Assessment of WNT/FZD selectivity and receptor conformational dynamics with FZD biosensors

After confirming the fidelity of all four FZD-cpGFP biosensors in uncovering WNT-3A/receptor interaction, we aimed to employ these optical tools to assess the interaction of FZDs with a panel of their endogenous ligands, applying commercially available, recombinant WNT preparations. We have previously used these WNT preparations at different occasions and in different cell systems ranging from primary mouse microglia cells, N13 microglia-like cells, and different HEK293 cells in order to characterize their activity in diverse biochemical and cell biological readouts (Arthofer et al., 2016; Dijksterhuis et al., 2015; Halleskog et al., 2011, 2012; Hot et al., 2017; Kilander et al., 2011, 2014a, 2014b). We stimulated the stable cell lines expressing either FZD_4-, FZD_5-, FZD_6-or FZD_7-cpGFP with increasing concentrations of WNT-3A and WNT-5A, and five additional recombinant WNTs (WNT-5B, -7A, -10B, -11, -16B) to examine WNT/FZD selectivity and efficacy in a downstream signaling-independent manner. These experiments revealed intriguing and unexpected patterns of WNT-induced conformational dynamics in FZDs (Fig. 5, Table 1). Most importantly, the FZD-cpGFP biosensors uncovered WNT-specific EC_{50} values at different receptors in the lower nanomolar range (Table 1). For instance, while WNT-3A (Fig. 5A, H, O, V) and WNT-7A (Fig. 5D, K, R, Y) induced conformational changes with similar potencies across all four FZD biosensors, WNT-5B solely yielded a saturating concentration-response curve at FZD_7 (Fig. 5C, J, Q, X). These unexpected findings indicate that whereas some WNTs (e.g. WNT-3A and WNT-7A) exhibit rather promiscuous coupling to all four homology clusters of class F, others, such as WNT-5B, selectively bind to individual FZD paralogs to induce receptor conformational changes.

Furthermore, we also observed intriguing amplitudes of the fluorescent response with several WNT/FZD combinations (of note, signal amplitudes should only be compared at the same FZD biosensors since the different probes show altering sensitivities as outlined in Fig. 4D). For instance, WNT-3A, WNT-5A and WNT-7A induced distinct FZD_4-cpGFP fluorescent responses at saturating ligand concentrations (Fig. 5A, B, D, Fig. S4). Moreover, WNT-16B (Fig. 5U) and WNT-11 (Fig. 5AA) even reduced the fluorescence intensity of cpGFP at FZD_6- and FZD_7-cpGFP, respectively. These signals are suggestive of distinct cpGFP conformational states resulting from varying receptor conformations, similar to what was previously described in other GPCR families (Hoffmann et al., 2012; Lane et al., 2020; Nikolaev et al., 2006; Picard et al., 2018; Schihada et al., 2018, 2020; Vilardaga et al., 2005).

4. Discussion

Ten distinct FZDs present the prime targets of 19 mammalian WNTs and mediate their (patho)physiological effects across the plasma membrane. Despite the crucial relevance of WNT/FZD signaling during embryonic development or tumorigenesis, little is known about the molecular mechanisms underlying WNT signaling via FZDs and the biological significance of individual ligand/receptor complexes. Studying these events with high spatial and temporal resolution has been hampered by a lack of appropriate technologies that quantify WNT/FZD interaction independently from downstream signaling. In the present study, we addressed this limitation by developing conformational FZD biosensors representing each of the four FZD homology clusters allowing to assess the conformational changes of FZDs upon WNT engagement in real time in living cells. These optical tools enabled us to examine receptor selectivity and potency of seven recombinant WNTs in a medium-throughput assay format.

This technological advancement can be harnessed in future studies to explore WNT/FZD pharmacology with improved throughput and accuracy since the conformational response of FZDs represents the most unbiased way to assess the interaction of WNTs with FZDs. While pathway-dependent readouts, such as the β-catenin-dependent TOP-Flash assay, solely characterize ligands based on their ability to promote this specific signaling cascade (e.g. WNT-3A but not WNT-5A), FZD-cpGFP sensors respond to ligands independently of their preferred signaling pathway. Application of this sensor principle to the other class F receptors and further refinement of the experimental setup by, for instance, establishing a membrane-based assay in 384-well plates, would result in an attractive screening platform to test efficiently an extensive small molecule library for FZD-targeting entities.

Besides the technical progress implicated in the development of these FZD biosensors, we further provide important biological insights that are of high relevance for our understanding of WNT/FZD pharmacology. In line with previous findings from our group (Kozielewicz et al., 2020; Wright et al., 2018) and molecular dynamics simulations (Yang et al., 2018), we demonstrate that FZDs undergo conformational rearrangements upon ligand engagement reminiscent of class A and B GPCRs. Furthermore, we show, for the first time, that these conformational

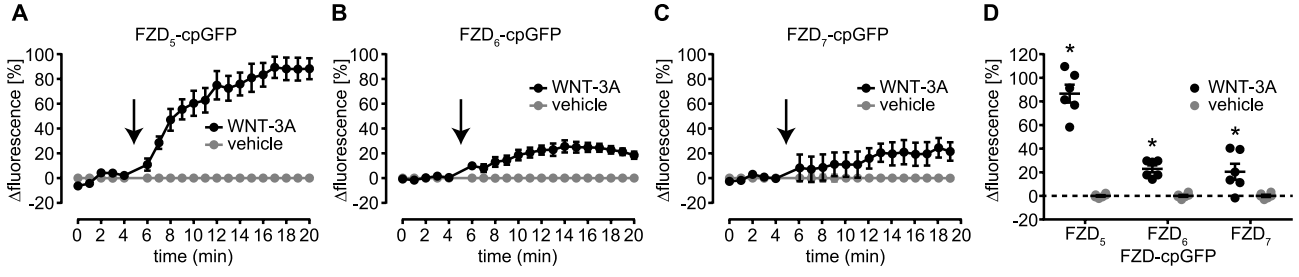

Fig. 4. Validation of $FZD_{5/6/7}$-cpGFP biosensors. (**A-C**) Fluorescence time-courses of FZD_5- (**A**), FZD_6- (**B**) and FZD_7-cpGFP (**C**) upon stimulation with 3 μg/mL of recombinant WNT-3A. The arrows indicate the timepoint of WNT or vehicle addition. (**D**) Fluorescence response induced by 3 μg/mL WNT-3A after 10 min incubation time. All experiments were performed using HEK293A cells stably expressing the indicated FZD biosensor. Data show mean ± s.e.m. of three independent experiments. Statistical significance in (D) was tested applying two-way ANOVA followed by Sidak's multiple comparison test against the respective vehicle control. $p < 0.05$. Assessment of WNT/FZD selectivity and conformational dynamics with FZD biosensors.

Table 1
Efficacies and potencies of recombinant WNTs on FZD-cpGFP biosensors.

	FZD_4-cpGFP			FZD_5-cpGFP			FZD_6-cpGFP			FZD_7-cpGFP		
	$EC_{50} \pm$ s.e.m. [ng/mL]	$pEC_{50} \pm$ s.e.m.[a]	$E_{max} \pm$ s.e.m. [%]	$EC_{50} \pm$ s.e.m. [ng/mL]	$pEC_{50} \pm$ s.e.m.[a]	E_{max} [%]	$EC_{50} \pm$ s.e.m. [ng/mL]	$pEC_{50} \pm$ s.e.m.[a]	E_{max} [%]	$EC_{50} \pm$ s.e.m. [ng/mL]	$pEC_{50} \pm$ s.e.m.[a]	E_{max} [%]
WNT-3A	2193 ± 130	7.25 ± 0.03	58 ± 3	1223 ± 117	7.51 ± 0.06	79 ± 4	1031 ± 264	7.59 ± 0.11	35 ± 5	1001 ± 357	7.60 ± 0.13	24 ± 4
WNT-5A	1652 ± 182	7.41 ± 0.05	42 ± 3	>6000	<6.9	n.a.	995 ± 676	7.62 ± 0.22	45 ± 10	>6000	<6.9	n.a.
WNT-5B	>6000	<6.9	n.a.	3272 ± 8144	7.09 ± 0.53	−30 ± 25	>6000	<6.9	n.a.	327 ± 253	8.10 ± 0.25	28 ± 6
WNT-7A	1551 ± 231	7.40 ± 0.06	88 ± 6	1583 ± 207	7.39 ± 0.05	81 ± 7	3334 ± 710	7.07 ± 0.13	49 ± 9	2919 ± 806	7.12 ± 0.10	29 ± 9
WNT-10B	>6000	<6.9	n.a.	>6000	<6.9	n.a.	>6000	<6.9	n.a.	>6000	<6.9	n.a.
WNT-11	3637 ± 5247	7.03 ± 0.39	−16 ± 17	2004 ± 4490	7.29 ± 0.51	−6 ± 6	>6000	<6.9	n.a.	1827 ± 1409	7.33 ± 0.25	−8 ± 4
WNT-16B	>6000	<6.9	n.a.	>6000	<6.9	n.a.	3585 ± 3852	7.06 ± 0.32	−13 ± 12	>6000	<6.9	n.a.

n.a.: not applicable since curve could not be fitted or did not yield computable saturation. Of note, different E_{max} values for the same WNT on distinct FZD subtypes can emerge from distinct maximal amplitudes of the biosensors. Therefore, E_{max} values should only be compared at the same FZD subtype.

[a] Molar masses of WNTs were taken from https://www.uniprot.org/ for EC_{50} conversion from ng/mL to nM: WNT-3A = 39,365 Da; WNT-5A = 42,339 Da; WNT-5B = 40,323 Da; WNT-7A = 39,005 Da; WNT-10B = 43,000 Da; WNT-11 = 39,179 Da; WNT-16B = 40,690 Da; pEC_{50} values were calculated from the computed EC_{50} values in mol/L.

dynamics do not depend upon interaction of FZDs with the WNT-coreceptors LRP5/6, which are necessary for WNT signaling through β-catenin. This result stands in contrast to a recent mutagenesis-based investigation of FZD/β-catenin signaling (Tsutsumi et al., 2020). In that study, WNT-3A and a FZD/LRP cross-linking surrogate ligand induced the same pattern of β-catenin signaling, leading the authors to conclude that FZD agonists do not activate their receptors by eliciting a conformational change. However, our results provide strong evidence that WNTs do induce conformational changes in FZDs, which is furthermore in strong agreement with the WNT-induced recruitment of mini G proteins, serving as conformational sensors for the active receptor, to FZDs (Wright et al., 2019). Furthermore, WNT-induced conformational dynamics were reported already for FZD_5 using an intramolecular FRET sensor (Wright et al., 2018). However, our current data do not allow to conclude that the conformational rearrangement in FZDs is required for this specific signaling pathway, i.e. DVL-mediated, β-catenin stabilization and gene transcription. In fact, WNT-3A also dissociates pre-assembled inactive state FZD_4 complexes with $G_{\alpha 12}$ proteins on the surface of living cells, to signal through RHO GTPase-dependent pathways (Arthofer et al., 2016). This, and potentially other FZD_4-mediated downstream pathways such as PCP-like signaling, might depend on the WNT-3A-mediated conformational change in FZD_4 that we detected even in presence of DKK1. These controversies underline the importance to appreciate the diverse signaling portfolio of the WNT/FZD system in order to attain a better understanding of these fundamental processes.

Besides these mechanistic insights into the agonist-induced dynamics of FZD conformation, our study further sheds light on the selectivity of WNT/FZD interactions. For instance, while WNT-3A, WNT-5A and WNT-7A evoked conformational responses in all four FZD homology clusters, WNT-5B selectively interacted with FZD_7. While very limited interaction data is available for WNT-5B (Dijksterhuis et al., 2014), a similar promiscuous interaction pattern of WNT-3A and WNT-5A has been reported based on their binding to soluble FZD CRDs (Dijksterhuis et al., 2015) and β-catenin reporter gene responses in HEK293 cells (Voloshanenko et al., 2017). Importantly, these results need to be interpreted in light of the specific co-receptor environment on the surface of HEK293 cells. As highlighted in a seminal study describing the role of co-receptors for WNT/FZD selectivity (Eubelen et al., 2018), endogenous expression levels of, for instance, ADGRA2 and RECK assist the interaction of WNTs with FZDs. These aspects need to be taken into consideration when ligand/receptor interaction patterns are compared between different host cell test systems. Additionally, secreted regulators of WNT signaling such as SFRPs, WIF-1, DKKs and TIKI1 modulate the pharmacological ligand properties of WNTs (and therefore potentially their selectivity profiles). On the other hand, our FZD sensor toolbox represents a suitable platform to examine the modulation of selected ligand/receptor pairings by these secreted biomolecules in order to deepen our understanding of this complex regulatory network.

Lastly, and probably most intriguingly from a pharmacological perspective, we monitored distinct amplitudes of the WNT-induced fluorescent signals of the FZD biosensors. This was not only apparent for WNT-3A and WNT-5A eliciting only about 40–60% of the WNT-7A-mediated response in FZD_4, but was most striking for WNT-11/FZD_7 and WNT-16B/FZD_6, which even showed reduced fluorescence signals at saturating ligand concentrations. The emission intensity of cpGFP depends on its structural organization and is therefore directly affected by, for instance, subtle but distinct twists of the flanking transmembrane helices 5 and 6. As it is well-accepted for class A, B and C GPCRs, these heptahelical proteins do not only switch between a single on or off state, but are able to adopt multiple intermediate conformations that underline distinct signaling functionalities (Smith et al., 2018). We therefore hypothesize that the varying amplitudes of the WNT-induced FZD-cpGFP responses at saturating ligand concentrations reflect distinct receptor conformational states. Follow-up studies are needed to assess the importance of these different conformations for signal initiation and pathway selectivity.

5. Conclusions

In summary, we present the design and validation of a panel of FZD conformational biosensors covering all four homology clusters of class F GPCRs. Exemplified with 28 distinct WNT/FZD pairs, we demonstrate how these sensors can be employed for a comprehensive mapping of the 190 possible WNT/FZD combinations and to screen chemical libraries for FZD-targeting compounds with drug-like properties. Our findings also provide unprecedented insights into the mechanistic basis of WNT interaction with their primary receptors, allowing for a deeper understanding of the complexity of the WNT/FZD signaling system, which has substantial implications for numerous biological processes in health and disease.

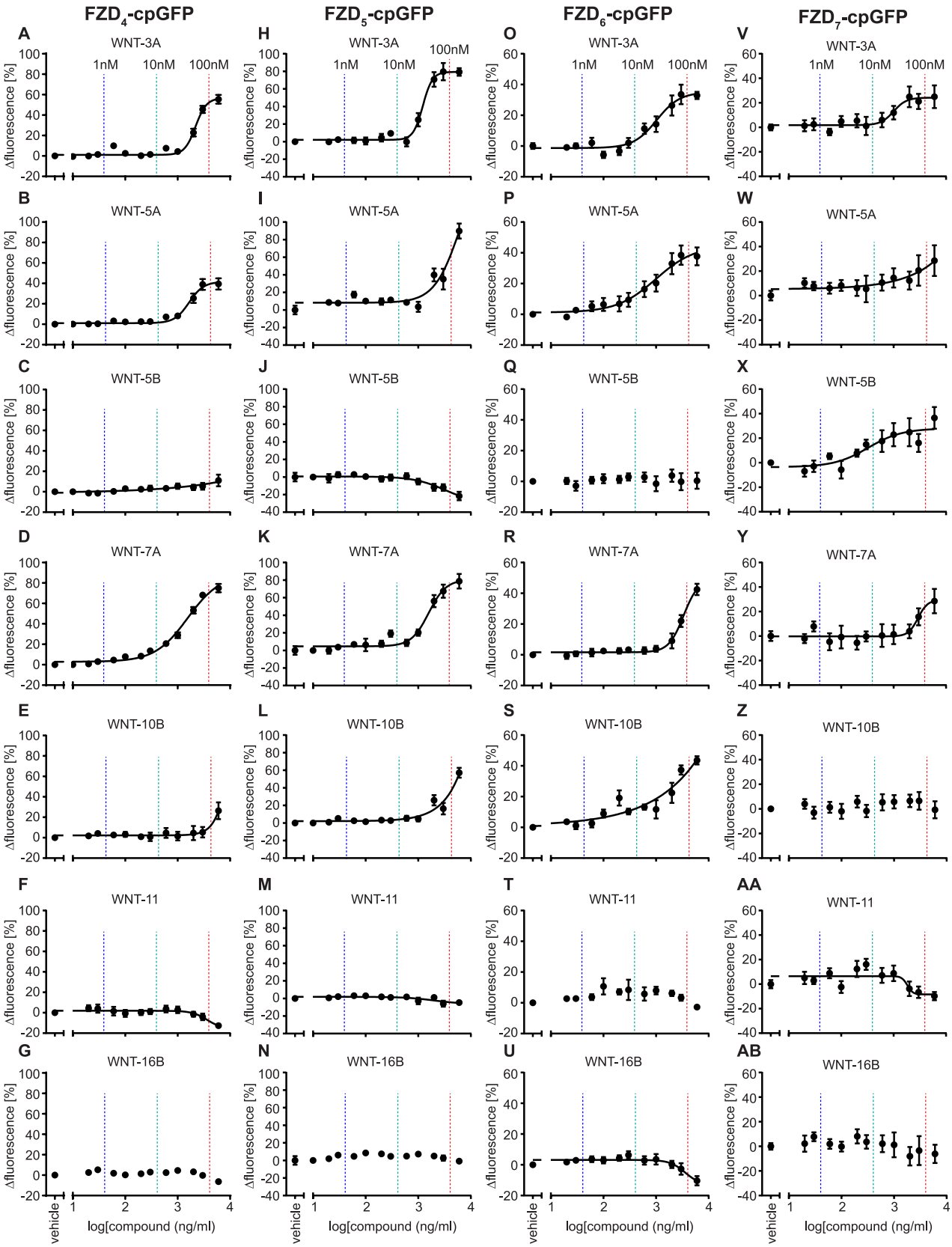

Fig. 5. Assessment of WNT/FZD selectivity and efficacy. Concentration-response curves of seven recombinant WNTs on HEK293A cells stably expressing FZD_4-cpGFP (**A-G**), FZD_5-cpGFP (**H–N**), FZD_6-cpGFP (**O–U**) or FZD_7-cpGFP (**V-AB**). Data show mean ± s.e.m. of three to six independent experiments. The dotted vertical lines were employed to indicate ligand concentrations in nM units and ease comparison with data from other studies. See also Table 1.

Declaration of competing interest

The authors declare that they have no known competing financial interests or personal relationships that could have appeared to influence the work reported in this paper.

Acknowledgments

We thank Anna Krook for access to the CLARIOstar plate reader, Thomas P. Sakmar (The Rockefeller University, NYC, USA) for providing the plasmid encoding HA-tagged synthetic FZD_5 and Benoit Vanhollebeke (Université Libre de Bruxelles, Gosselies, Belgium) for the ΔFZD_{1-10} HEK293 cells.

Appendix A. Supplementary data

Supplementary data to this article can be found online at https://doi.org/10.1016/j.bios.2020.112948.

Funding sources

The work was supported by the Deutsche Forschungsgemeinschaft (DFG, German Research Foundation – 427840891; KO 5463/1-1) and grants from Karolinska Institutet, the Swedish Research Council (2017–04676; 2019–01190), the Swedish Cancer Society (CAN2017/561), the Novo Nordisk Foundation (NNF17OC0026940, NNF19OC0056122, NNF20OC0063168), Wenner-Gren Foundations (UPD2018-0064), Emil and Wera Cornells Stiftelse.

The funding sources were not involved in the study design; in the collection, analysis and interpretation of data; in the writing of the article; and in the decision to submit the article for publication.

References

Arthofer, E., Hot, B., Petersen, J., Strakova, K., Jager, S., Grundmann, M., Kostenis, E., Gutkind, J.S., Schulte, G., 2016. WNT stimulation dissociates a frizzled 4 inactive-state complex with galpha12/13. Mol. Pharmacol. 90, 447–459.

Bhanot, P., Brink, M., Samos, C.H., Hsieh, J.C., Wang, Y., Macke, J.P., Andrew, D., Nathans, J., Nusse, R., 1996. A new member of the frizzled family from Drosophila functions as a Wingless receptor. Nature 382, 225–230.

Bilic, J., Huang, Y.L., Davidson, G., Zimmermann, T., Cruciat, C.M., Bienz, M., Niehrs, C., 2007. Wnt induces LRP6 signalosomes and promotes dishevelled-dependent LRP6 phosphorylation. Science 316, 1619–1622.

Blagodatski, A., Poteryaev, D., Katanaev, V.L., 2014. Targeting the Wnt pathways for therapies. Mol Cell Ther 2, 28.

Bowin, C.F., Inoue, A., Schulte, G., 2019. WNT-3A-induced beta-catenin signaling does not require signaling through heterotrimeric G proteins. J. Biol. Chem. 294, 11677–11684.

Bryja, V., Gradl, D., Schambony, A., Arenas, E., Schulte, G., 2007. Beta-arrestin is a necessary component of Wnt/beta-catenin signaling in vitro and in vivo. Proc. Natl. Acad. Sci. U. S. A. 104, 6690–6695.

Bryja, V., Schambony, A., Cajanek, L., Dominguez, I., Arenas, E., Schulte, G., 2008. Beta-arrestin and casein kinase 1/2 define distinct branches of non-canonical WNT signalling pathways. EMBO Rep. 9, 1244–1250.

Byrne, E.F.X., Sircar, R., Miller, P.S., Hedger, G., Luchetti, G., Nachtergaele, S., Tully, M. D., Mydock-McGrane, L., Covey, D.F., Rambo, R.P., et al., 2016. Structural basis of Smoothened regulation by its extracellular domains. Nature 535, 517–522.

Clevers, H., Nusse, R., 2012. Wnt/beta-catenin signaling and disease. Cell 149, 1192–1205.

De Lean, A., Stadel, J.M., Lefkowitz, R.J., 1980. A ternary complex model explains the agonist-specific binding properties of the adenylate cyclase-coupled beta-adrenergic receptor. J. Biol. Chem. 255, 7108–7117.

DeBruine, Z.J., Xu, H.E., Melcher, K., 2017. Assembly and architecture of the Wnt/beta-catenin signalosome at the membrane. Br. J. Pharmacol. 174, 4564–4574.

Dijksterhuis, J.P., Baljinnyam, B., Stanger, K., Sercan, H.O., Ji, Y., Andres, O., Rubin, J.S., Hannoush, R.N., Schulte, G., 2015. Systematic mapping of WNT-FZD protein interactions reveals functional selectivity by distinct WNT-FZD pairs. J. Biol. Chem. 290, 6789–6798.

Dijksterhuis, J.P., Petersen, J., Schulte, G., 2014. WNT/Frizzled signalling: receptor-ligand selectivity with focus on FZD-G protein signalling and its physiological relevance: IUPHAR Review 3. Br. J. Pharmacol. 171, 1195–1209.

Eubelen, M., Bostaille, N., Cabochette, P., Gauquier, A., Tebabi, P., Dumitru, A.C., Koehler, M., Gut, P., Alsteens, D., Stainier, D.Y.R., et al., 2018. A molecular mechanism for Wnt ligand-specific signaling. Science 361.

Feng, J., Zhang, C., Lischinsky, J.E., Jing, M., Zhou, J., Wang, H., Zhang, Y., Dong, A., Wu, Z., Wu, H., et al., 2019. A genetically encoded fluorescent sensor for rapid and specific in vivo detection of norepinephrine. Neuron 102, 745–761 e748.

Garcia de Herreros, A., Dunach, M., 2019. Intracellular signals activated by canonical wnt ligands independent of GSK3 inhibition and beta-catenin stabilization. Cells 8 (10).

Grainger, S., Willert, K., 2018. Mechanisms of Wnt Signaling and Control. Wiley Interdiscip Rev Syst Biol Med, p. e1422.

Grumolato, L., Liu, G., Mong, P., Mudbhary, R., Biswas, R., Arroyave, R., Vijayakumar, S., Economides, A.N., Aaronson, S.A., 2010. Canonical and noncanonical Wnts use a common mechanism to activate completely unrelated coreceptors. Genes Dev. 24, 2517–2530.

Halleskog, C., Dijksterhuis, J.P., Kilander, M.B., Becerril-Ortega, J., Villaescusa, J.C., Lindgren, E., Arenas, E., Schulte, G., 2012. Heterotrimeric G protein-dependent WNT-5A signaling to ERK1/2 mediates distinct aspects of microglia proinflammatory transformation. J. Neuroinflammation 9, 111.

Halleskog, C., Mulder, J., Dahlstrom, J., Mackie, K., Hortobagyi, T., Tanila, H., Kumar Puli, L., Farber, K., Harkany, T., Schulte, G., 2011. WNT signaling in activated microglia is proinflammatory. Glia 59, 119–131.

Hoffmann, C., Nuber, S., Zabel, U., Ziegler, N., Winkler, C., Hein, P., Berlot, C.H., Bunemann, M., Lohse, M.J., 2012. Comparison of the activation kinetics of the M3 acetylcholine receptor and a constitutively active mutant receptor in living cells. Mol. Pharmacol. 82, 236–245.

Hot, B., Valnohova, J., Arthofer, E., Simon, K., Shin, J., Uhlen, M., Kostenis, E., Mulder, J., Schulte, G., 2017. FZD10-Galpha13 signalling axis points to a role of FZD10 in CNS angiogenesis. Cell. Signal. 32, 93–103.

Hsieh, J.C., Rattner, A., Smallwood, P.M., Nathans, J., 1999. Biochemical characterization of Wnt-frizzled interactions using a soluble, biologically active vertebrate Wnt protein. Proc. Natl. Acad. Sci. U. S. A. 96, 3546–3551.

Hua, Y., Yang, Y., Li, Q., He, X., Zhu, W., Wang, J., Gan, X., 2018. Oligomerization of Frizzled and LRP5/6 protein initiates intracellular signaling for the canonical WNT/beta-catenin pathway. J. Biol. Chem. 293, 19710–19724.

Janda, C.Y., Waghray, D., Levin, A.M., Thomas, C., Garcia, K.C., 2012. Structural basis of wnt recognition by frizzled. Science 337, 59–64.

Jing, M., Zhang, P., Wang, G., Feng, J., Mesik, L., Zeng, J., Jiang, H., Wang, S., Looby, J. C., Guagliardo, N.A., et al., 2018. A genetically encoded fluorescent acetylcholine indicator for in vitro and in vivo studies. Nat. Biotechnol. 36, 726–737.

Kilander, M.B., Dahlstrom, J., Schulte, G., 2014a. Assessment of Frizzled 6 membrane mobility by FRAP supports G protein coupling and reveals WNT-Frizzled selectivity. Cell. Signal. 26, 1943–1949.

Kilander, M.B., Halleskog, C., Schulte, G., 2011. Recombinant WNTs differentially activate beta-catenin-dependent and -independent signalling in mouse microglia-like cells. Acta Physiol. 203, 363–372.

Kilander, M.B., Petersen, J., Andressen, K.W., Ganji, R.S., Levy, F.O., Schuster, J., Dahl, N., Bryja, V., Schulte, G., 2014b. Disheveled regulates precoupling of heterotrimeric G proteins to Frizzled 6. Faseb. J. 28, 2293–2305.

Kim, G.H., Her, J.H., Han, J.K., 2008. Ryk cooperates with Frizzled 7 to promote Wnt11-mediated endocytosis and is essential for Xenopus laevis convergent extension movements. J. Cell Biol. 182, 1073–1082.

Koval, A., Katanaev, V.L., 2012. Platforms for high-throughput screening of Wnt/Frizzled antagonists. Drug Discov. Today 17, 1316–1322.

Kozielewicz, P., Turku, A., Bowin, C.F., Petersen, J., Valnohova, J., Canizal, M.C.A., Ono, Y., Inoue, A., Hoffmann, C., Schulte, G., 2020. Structural insight into small molecule action on Frizzleds. Nat. Commun. 11, 414.

Kozielewicz, P., Turku, A., Schulte, G., 2019. Molecular pharmacology of class F receptor activation. Mol. Pharmacol. 97 (2), 62–71.

Lane, J.R., Abramyan, A.M., Adhikari, P., Keen, A.C., Lee, K.H., Sanchez, J., Verma, R.K., Lim, H.D., Yano, H., Javitch, J.A., et al., 2020. Distinct inactive conformations of the dopamine D2 and D3 receptors correspond to different extents of inverse agonism. Elife 9.

Larkin, M.A., Blackshields, G., Brown, N.P., Chenna, R., McGettigan, P.A., McWilliam, H., Valentin, F., Wallace, I.M., Wilm, A., Lopez, R., et al., 2007. Clustal W and clustal X version 2.0. Bioinformatics 23, 2947–2948.

Lohse, M.J., Nuber, S., Hoffmann, C., 2012. Fluorescence/bioluminescence resonance energy transfer techniques to study G-protein-coupled receptor activation and signaling. Pharmacol. Rev. 64, 299–336.

Nikolaev, V.O., Hoffmann, C., Bunemann, M., Lohse, M.J., Vilardaga, J.P., 2006. Molecular basis of partial agonism at the neurotransmitter alpha2A-adrenergic receptor and Gi-protein heterotrimer. J. Biol. Chem. 281, 24506–24511.

Nusse, R., Clevers, H., 2017. Wnt/beta-Catenin signaling, disease, and emerging therapeutic modalities. Cell 169, 985–999.

Patriarchi, T., Cho, J.R., Merten, K., Howe, M.W., Marley, A., Xiong, W.H., Folk, R.W., Broussard, G.J., Liang, R., Jang, M.J., et al., 2018. Ultrafast neuronal imaging of dopamine dynamics with designed genetically encoded sensors. Science 360.

Picard, L.P., Schonegge, A.M., Lohse, M.J., Bouvier, M., 2018. Bioluminescence resonance energy transfer-based biosensors allow monitoring of ligand- and transducer-mediated GPCR conformational changes. Commun Biol 1, 106.

Qi, X., Friedberg, L., De Bose-Boyd, R., Long, T., Li, X., 2020. Sterols in an intramolecular channel of Smoothened mediate Hedgehog signaling. Nat. Chem. Biol. 16 (12), 1368–1375.

Qi, X., Liu, H., Thompson, B., McDonald, J., Zhang, C., Li, X., 2019. Cryo-EM structure of oxysterol-bound human Smoothened coupled to a heterotrimeric Gi. Nature 571, 279–283.

Schihada, H., Ma, X., Zabel, U., Vischer, H.F., Schulte, G., Leurs, R., Pockes, S., Lohse, M. J., 2020. Development of a conformational histamine H3 receptor biosensor for the synchronous screening of agonists and inverse agonists. ACS Sens. 5 (6), 1734–1742.

Schihada, H., Vandenabeele, S., Zabel, U., Frank, M., Lohse, M.J., Maiellaro, I., 2018. A universal bioluminescence resonance energy transfer sensor design enables high-sensitivity screening of GPCR activation dynamics. Commun Biol 1, 105.
Schulte, G., 2010. International union of basic and clinical pharmacology. LXXX. The class frizzled receptors. Pharmacol. Rev. 62, 632–667.
Schulte, G., 2015. Frizzleds and WNT/beta-catenin signaling–The black box of ligand-receptor selectivity, complex stoichiometry and activation kinetics. Eur. J. Pharmacol. 763, 191–195.
Schulte, G., Wright, S.C., 2018. Frizzleds as GPCRs - more conventional than we thought! Trends Pharmacol. Sci. 39, 828–842.
Semenov, M.V., Habas, R., Macdonald, B.T., He, X., 2007. SnapShot: noncanonical wnt signaling pathways. Cell 131, 1378.
Shen, M.Y., Sali, A., 2006. Statistical potential for assessment and prediction of protein structures. Protein Sci. 15, 2507–2524.
Smith, J.S., Lefkowitz, R.J., Rajagopal, S., 2018. Biased signalling: from simple switches to allosteric microprocessors. Nat. Rev. Drug Discov. 17, 243–260.
Sun, F., Zeng, J., Jing, M., Zhou, J., Feng, J., Owen, S.F., Luo, Y., Li, F., Wang, H., Yamaguchi, T., et al., 2018. A genetically encoded fluorescent sensor enables rapid and specific detection of dopamine in flies, fish, and mice. Cell 174, 481–496 e419.
Tsutsumi, N., Mukherjee, S., Waghray, D., Janda, C.Y., Jude, K.M., Miao, Y., Burg, J.S., Aduri, N.G., Kossiakoff, A.A., Gati, C., et al., 2020. Structure of human Frizzled5 by fiducial-assisted cryo-EM supports a heterodimeric mechanism of canonical Wnt signaling. Elife 9.
Valnohova, J., Kowalski-Jahn, M., Sunahara, R.K., Schulte, G., 2018. Functional dissection of the N-terminal extracellular domains of Frizzled 6 reveals their roles for receptor localization and Dishevelled recruitment. J. Biol. Chem. 293, 17875–17887.
van Amerongen, R., Mikels, A., Nusse, R., 2008. Alternative wnt signaling is initiated by distinct receptors. Sci. Signal. 1, re9.
Vilardaga, J.P., Bunemann, M., Krasel, C., Castro, M., Lohse, M.J., 2003. Measurement of the millisecond activation switch of G protein-coupled receptors in living cells. Nat. Biotechnol. 21, 807–812.
Vilardaga, J.P., Steinmeyer, R., Harms, G.S., Lohse, M.J., 2005. Molecular basis of inverse agonism in a G protein-coupled receptor. Nat. Chem. Biol. 1, 25–28.
Voloshanenko, O., Gmach, P., Winter, J., Kranz, D., Boutros, M., 2017. Mapping of Wnt-Frizzled interactions by multiplex CRISPR targeting of receptor gene families. Faseb. J. 31, 4832–4844.
Wang, C., Wu, H., Evron, T., Vardy, E., Han, G.W., Huang, X.P., Hufeisen, S.J., Mangano, T.J., Urban, D.J., Katritch, V., et al., 2014. Structural basis for Smoothened receptor modulation and chemoresistance to anticancer drugs. Nat. Commun. 5, 4355.
Wang, Y., Chang, H., Rattner, A., Nathans, J., 2016. Frizzled receptors in development and disease. Curr. Top. Dev. Biol. 117, 113–139.
Webb, B., Sali, A., 2014. Protein structure modeling with MODELLER. Methods Mol. Biol. 1137, 1–15.
Wesslowski, J., Kozielewicz, P., Wang, X., Cui, H., Schihada, H., Kranz, D., Karuna, M.P., Levkin, P., Gross, J.C., Boutros, M., et al., 2020. eGFP-tagged Wnt-3a enables functional analysis of Wnt trafficking and signaling and kinetic assessment of Wnt binding to full-length Frizzled. J. Biol. Chem. 295, 8759–8774.
Wright, S.C., Canizal, M.C.A., Benkel, T., Simon, K., Le Gouill, C., Matricon, P., Namkung, Y., Lukasheva, V., Konig, G.M., Laporte, S.A., et al., 2018. FZD5 is a Galphaq-coupled receptor that exhibits the functional hallmarks of prototypical GPCRs. Sci. Signal. 11.
Wright, S.C., Kozielewicz, P., Kowalski-Jahn, M., Petersen, J., Bowin, C.F., Slodkowicz, G., Marti-Solano, M., Rodriguez, D., Hot, B., Okashah, N., et al., 2019. A conserved molecular switch in Class F receptors regulates receptor activation and pathway selection. Nat. Commun. 10, 667.
Wu, C.H., Nusse, R., 2002. Ligand receptor interactions in the Wnt signaling pathway in Drosophila. J. Biol. Chem. 277, 41762–41769.
Yang, S., Wu, Y., Xu, T.H., de Waal, P.W., He, Y., Pu, M., Chen, Y., DeBruine, Z.J., Zhang, B., Zaidi, S.A., et al., 2018. Crystal structure of the Frizzled 4 receptor in a ligand-free state. Nature 560, 666–670.
Yang, Y., Mlodzik, M., 2015. Wnt-Frizzled/planar cell polarity signaling: cellular orientation by facing the wind (Wnt). Annu. Rev. Cell Dev. Biol. 31, 623–646.
Yu, H., Ye, X., Guo, N., Nathans, J., 2012. Frizzled 2 and frizzled 7 function redundantly in convergent extension and closure of the ventricular septum and palate: evidence for a network of interacting genes. Development 139, 4383–4394.